Structural Integrity Analysis of a Two-Pole Synchronous Reluctance Machine with Non-circular Shaft

Didem Tekgun
Department of Electrical & Electronics Engineering
Abdullah Gul University
Kayseri, TURKEY
didem.tekgun@agu.edu.tr

Burak Tekgun
Department of Electrical & Electronics Engineering
Abdullah Gul University
Kayseri, TURKEY
burak.tekgun@agu.edu.tr

Irfan Alan
Department of Electrical & Electronics Engineering
Abdullah Gul University
Kayseri, TURKEY
irfan.alan@agu.edu.tr

2023 5th Global Power, Energy and Communication Conference (GPECOM) | 979-8-3503-0198-4/23/$31.00 ©2023 IEEE | DOI: 10.1109/GPECOM58364.2023.10175767

***Abstract*— This paper investigates the structural strength of a 6-inch diameter, two-pole, 4 kW line start synchronous reluctance machine (LS-SynRM) designed with a new non-circular shaft structure that serves as a pump motor. Flux paths on the rotor are widened while narrowing down the shaft of the motor on the q-axis to improve the motor efficiency. By using this method, a wider path is created for the flux in the d-axis. As a result, the inductance in the d-axis, the ratio of inductance between the d-axis and q-axis (referred to as saliency ratio), and the difference in inductance between the d-axis and q-axis are all amplified. To evaluate the structural strength of the machine, a series of analyses are conducted, including modal, harmonic, and static examination on the rotor using ANSYS Structural. The findings indicate that to prevent redundant deformations and undesirable vibrations because of resonance, the maximum safe limit for shaft size reduction is determined as 8 mm.**

Keywords—synchronous reluctance machine, line start, non-circular shaft, structural integrity, ANSYS

I. INTRODUCTION

Currently, there is a global effort to reduce energy losses in order to preserve natural resources and decrease energy expenses. Electric motors are responsible for almost half of worldwide energy consumption, making it critical to improve their efficiency at both the national and global levels [1], [2]. In industrial settings, electric motors are frequently used for pumping petroleum products and underground water, but they may have low efficiency due to factors such as cost, design, and the use of inappropriate motor-pump configurations. However, Induction motors exhibit low efficiency, particularly when operating at power levels that are low to medium [3].

Permanent Magnet Synchronous Machine (PMSM) is becoming more popular as a replacement for Induction Motors (IMs) because of their higher power density and efficiency [4]. These benefits are attributed to the use of permanent magnets, which facilitate efficient power transfer by interacting with the stator's magnetic field. Nevertheless, PMSMs are notably more costly and necessitate power electronics drives for their operation. PMSMs with drive systems offer good performance, their cost is a limiting factor for their widespread use in submersible pump applications. Line Start PMSMs (LS-PMSMs) are available on the market and have a comparatively lower initial cost because the need for a drive cost is eliminated [5]. However, issues such as demagnetization during start-up, high expenses, and dependence on rare-earth magnet have compelled scientists to investigate other motor alternatives.

Synchronous Reluctance Motors (SynRMs) are making them a feasible substitute for Induction Motors (IMs) because of their high level of efficiency [6]. Nonetheless, like PMSMs, they need power electronic drives. A topology known as Line Start SynRM (LS-SynRM) has surfaced as a viable substitute for IMs to overcome this challenge. LS-SynRM merges the line start ability of squirrel cage IMs with the saliency torque of SynRMs while eliminating the necessity for rare earth permanent magnets. The rotor of LS-SynRM comprises a conductor bar structure that allows it to begin operating as an IM while preserving the salient rotor architecture of a SynRM. After reaching synchronous speed, LS-SynRM functions as a SynRM, relying exclusively on the saliency torque created by the rotor's flux barriers. As a result, there is zero loss at the conductor bars since there are no induced currents in them. Furthermore, SynRM provide higher power and torque density than IM [7]. LS-SynRM therefore presents an appealing and cost-effective option that is reliable and efficient, especially when compared to the expensive PMSMs and low-efficiency IMs [8]. However, running the motor in both asynchronous and synchronous operations can be a complicated process, with potential problems such as inability to catching synchronization and crawling that require careful investigation.

In the case of submersible pump applications, maintaining a satisfactory hydraulic efficiency becomes problematic when operating below 1800 rpm, resulting in a substantial reduction in the overall system efficiency. As a result, 2 pole machines are frequently favored for these applications because they operate at higher speeds ranging from 3000-3600 rpm with 50 or 60 Hz excitation frequency. There is limited research available in the literature about use of SynRM as a motor for submersible water pumps, most of the existing studies concentrate on 4 pole SynRM configurations to attain high levels of efficiency [9-11]. However, there are available a few studies that examine the use of 2 pole LS-SynRM as pump motors [12], [13].

The ratio of Ld/Lq is a significant factor in designing SynRM since the torque is mainly dependent on reluctance, which is influenced by the flux barrier position and shape. The Ld/Lq ratio can be affected by various parameters, including the number of flux barriers, poles, thickness and width of the barriers, and air gap length. However, achieving significant saliency can be challenging in two-pole SynRMs

due to a flux bottleneck created by its geometry on the rotor. A design and optimization of a two-pole, 4 kW, 6" LS-SynRM for use in down hole water pump applications is proposed in [14-16]. The studies employed a rapid optimization algorithm approach for the design and optimization of a two-pole LS-SynRM for submersible water pump applications. More details on the topology can be found in [17]. The objective was to improve the performance of the machine by narrowing the shaft on the q-axis, thereby expanding the flux paths on the rotor. Consequently, the d-axis path is broader, and inductance in the d-axis is raised, which leads to a greater Ld/Lq saliency ratio and inductance difference (Ld-Lq), resulting in improved efficiency and saliency torque. Nevertheless, it is crucial to take into account the impacts of the modified shaft configuration on the rotor's mechanical stability, vibrational characteristics, and distortions.

In this paper, structural strength of a two- pole LS-SynRM is investigated with a non-circular shaft structure. This study conducted a comprehensive analysis using Finite Element Analysis (FEA) to establish the maximum safe limits of the new shaft design. Moreover, it also investigates the natural frequencies and vibration behavior, considering manufacturing tolerances by defining axial misalignment. In order to guarantee the durability of the redesigned shaft structure, an evaluation of shear stress is carried out, taking into account the initial torque is several times of the rated value.

The subsequent sections of the paper are structured in the following manner: Section II presents an overview of the LS-SynRM structure, providing simplified explanations to facilitate better comprehension. In Section III, the designed LS-SynRM with the new shaft structure is analyzed in detail with a focus on its rotor dynamics, describing its distinct features and performance. Section IV of the paper presents the results of the rotor dynamics analysis of the LS-SynRM, demonstrating the motor's structural integrity level with the newly designed non-circular shaft. Finally, Section V provides a summary of the study's main findings and implications and presents the conclusions.

II. Structure of 2 pole LS-SynRM

The line start synchronous machines are combining the squirrel cage IM and synchronous machine. Likewise, LS-SynRM is incorporating multiple flux barriers in the rotor for generating reluctance torque, as well as conductor bars that produce induction torque during startup. Given exponential relationship between the pump load and speed, the submersible motor experiences a light load during startup and gradually reaches its rated load as the speed approaches synchronous speed. To achieve synchronization and generate the required torque, the induction torque must meet a certain threshold. The size of the rotor conductor bar's cross-sectional area plays a crucial role in achieving synchronization and must be calculated with precision. Moreover, the gap between the bars and the airgap should be selected in a way that helps in achieving synchronization [11].

After reaching the synchronous speed, the LS-SynRM shifts its torque production from induction torque to reluctance torque and functions as a SynRM in steady-state. Obtaining satisfactory Ld−Lq and Ld/Lq becomes challenging as narrow the flux paths due to bars inserted to rotor that is required for generating adequate startup torque. Nevertheless, it is important to optimize the sizes of both the flux carrier and barrier to achieve optimal performance.

III. Rotor Dynamics

Increasing the thickness of the flux barrier will result in a reduction of q-axis inductance, leading to an increase in Ld/Lq and Ld−Lq. However, this also results in a decrease in d-axis inductance since the thickness of the flux carrier is reduced. Hence, finding the ideal thickness and right balance for both the flux barriers and carriers is crucial, there is a tradeoff between the two. Conducting an optimization study is necessary to determine the optimal thickness for both components. This can be a challenging process, especially for designing two-pole motors, as the restricted area on the rotor q-axis, as illustrated in Fig. 1, poses an additional difficulty.

The study proposes widening the rotor lamination thickness on the q-axis with minimizing the size of shaft to determine the physical limits, as shown in Fig. 1. Consequently, a wider path is provided to the flux on rotor, which resulting in increased reluctance torque as the d-axis inductance and saliency increase.

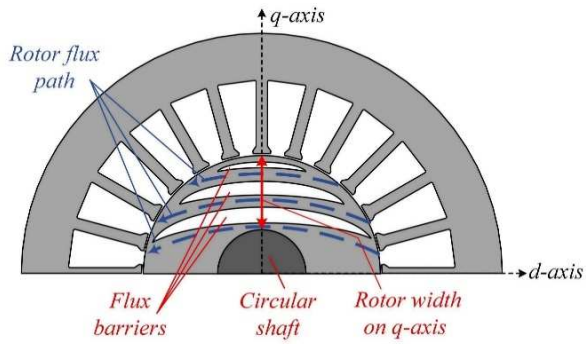

(a)

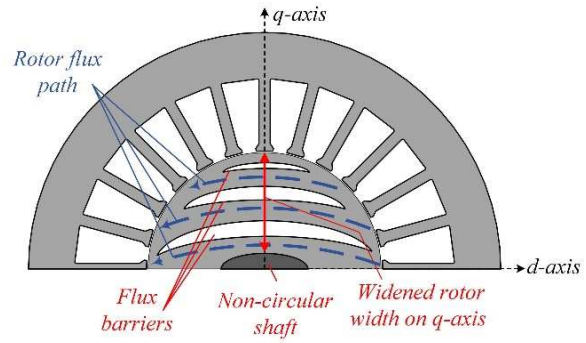

(b)

Fig.1. Two-pole SynRM rotor flux paths with (a) standard and (b) non-circular shafts.

IV. Structural Integrity Analysis and Results

The structural analysis of the proposed machine with the new non-circular shaft structure is conducted to determine its safe operational limits in terms of deformation and vibration while running at the rated speed.

The motor is subjected to a three-stage structural analysis. In the first stage, modal analysis is conducted for identifying the initial natural frequencies of the shafts with different size reduction in the q-axis (D_{OS}). This analysis helps in finding the acceptable limits of shaft reduction to be selected to prevent unwanted resonance related vibrations. Then,

harmonic analysis is performed to calculate the deformation and stress including fabrication imperfections in the rotor's geometry. Finally, static structural analysis is carried out to affirm the new structure can withstand the startup torque, which is three to five times greater than the rated torque. ANSYS Structural program provides an extensive array of features to analyze different phases of structural systems. The analysis of all stages is performed using ANSYS Structural.

First, a 3D model is created as the initial step of the analysis. Following this, the connections between components and the anchor points that provide support to the structure are defined. The geometry used for this analysis is made up of five components, including the squirrel cage rotor conductors, an upper circular shaft, a lower circular shaft, and a non-circular mid-section of the shaft. This configuration is depicted in Fig. 2. The rotor cage is well fitted to the main rotor body, creating a secure bond between all the components. The rotor is held in place by two sliding bearings which are inserted into the fixed motor body.

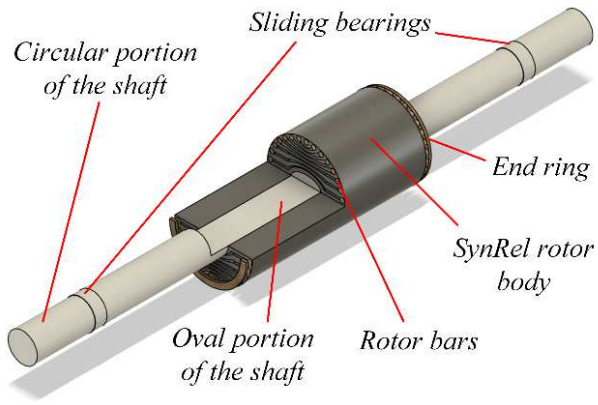

Fig.2. Structure of the rotor geometry of the proposed LS-SynRM.

To identify the natural vibration modes of the rotor's shape modal analysis is carried out [18]. Modal analysis enables observation of the material's response to various excitation frequencies. The analyses focus on D_{OS} (measurement of circular shaft size reduction in the q-axis) ranging from 0 to 10 mm to examine the degree to which the shaft can be reduced. In addition, the analysis takes into account the potential axis misalignment resulting from the manufacturing process.

The analysis is carried out up to 70 Hz, even though the maximum excitation frequency of a line start motor is 60 Hz. Table I presents the modal analysis results with a 0.1mm central misplacement at 70 Hz. The analysis found the first natural frequency (1st NF) of the rotor as 259 Hz when the shaft is a standard 25 mm circle. It is also observed that increasing the D_{OS} by 2 mm increments results in a decrease in the 1st NF.

In this article, the secure operational threshold for the 1st NF at twice the frequency of the excitation, implying that if the 1st NF exceeds twice the excitation frequency, it is possible to evade extreme deformations and vibrations. As the D_{OS} is fixed at 10 mm, the 1st NF is calculated as 99.82 Hz, that is lower than twice the frequency of the excitation. Consequently, the analysis concludes that the D_{OS} should be limited to 8 mm since the 1st NF occurs at 146.6Hz.

TABLE I. RESULTS BELONG TO THE MODAL ANALYSES

D_{OS} (mm)	First Natural Frequency (1NF) (Hz)
0	259.07
2	239.08
4	213.75
6	183.56
8	146.60
10	99.82

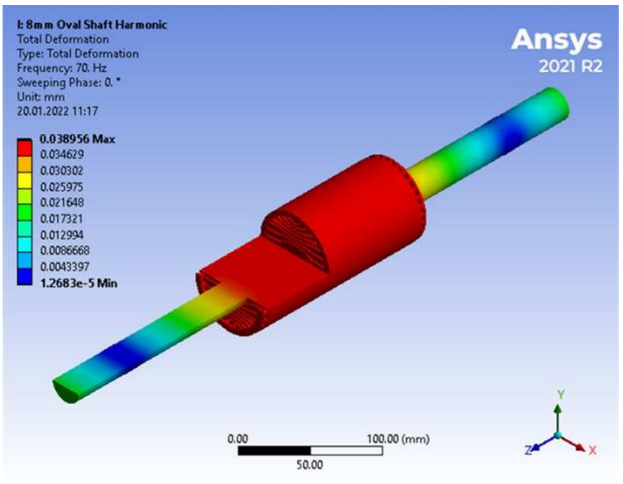

Fig. 3. Proposed motor total deformation with D_{OS} = 8 mm.

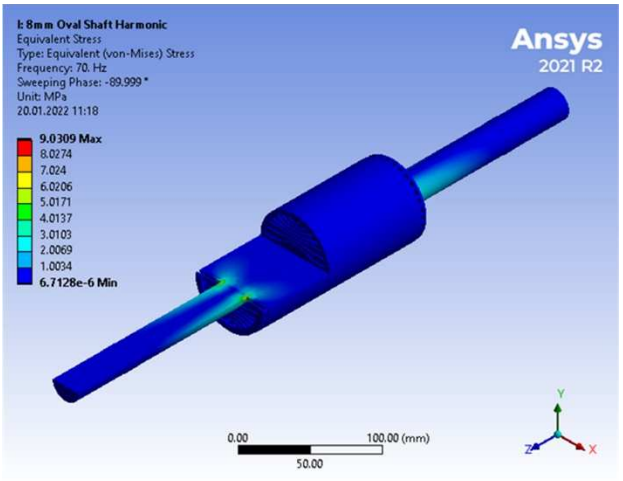

Fig. 4. Stress analysis results of the motor with D_{OS} = 8 mm

This analysis establishes a rotational motion applied to the rotor body, wherein the software computes material's deformation and stress at various excitation frequencies, taking into account the center of gravity, axial misalignment, and centrifugal force. Based on the results presented in Table II, both the maximum deformation and equivalent stress exhibit exponential growth as D_{OS} increases. When D_{OS} rises to 10 mm, an exponential increase in maximum deformation and equivalent stress is obtained. Therefore, the maximum acceptable D_{OS} limit is determined as 8 mm, as indicated in Fig. 3, where the maximum calculated deformation is 0.0389 mm, which is far below the motor's airgap length of 0.35 mm. Fig. 4 demonstrates that the highest values appear on the intersection of the non-circular and circular shaft regions.

To ensure structural stability, a specific material's yield stress should be greater than the stress experienced by the rotor. In this case, electric steel's yield stress, 350 MPa, should not be exceeded [19]. The calculated equivalent stress on the rotor is found to be 9.031 MPa when the D_{OS} is 8 mm, further confirming the design utilizing is secure and satisfactory.

TABLE II. RESULTS OF THE HARMONIC ANALYSES

D_{OS} (mm)	Equivalent Stress (MPa)	Maximum Deformation (mm)
0	2.716	0.0073
2	4.944	0.0123
4	5.456	0.0158
6	6.707	0.0226
8	9.031	0.0388
10	26.775	0.1195

Finally, the shear stress is calculated while the rotor is motionless with a torque that is five times greater than the rated one. Even though the previous analyses confirmed that selecting the D_{OS} as 8 mm is safe, shear stress was calculated for D_{OS} values of 0, 5, and 8 mm to examine the impact. Based on the results, the shear stress gradually rises with the D_{OS} length. The maximum value is recorded as 102.48 MPa and the total deformation value is calculated as 0.2 mm. Thus, these results lie within the acceptable tolerance limits even when the shaft is subjected to 5 times the rated torque. Table III presents the analysis results.

TABLE III. ANALYSES RESULTS FOR STARTING TORQUE

Analysis Type / D_{OS} (mm)	Max. shear stress (MPa)	Equivalent stress (MPa)	Total deformation (mm)
0	49.978	86.556	0.0225
5	51.279	87.235	0.0228
8	102.48	182.03	0.2000

The structural analyses indicate that reducing the shaft diameter on the q-axis up to 8 mm is safe and permissible.

After determining the safe shaft size reduction length as 8 mm along the q-axis, LS-SynRM is analyzed with circular shaft and non-circular shafts using ANSYS Electromagnetics Suite's Maxwell 2D module. According to the results, efficiency is recorded as 85.81 % when motor has circular shaft (D_{OS} = 0). On the other hand, the efficiency with D_{OS} = 5 mm is obtained as 86.65 % while D_{OS} = 8 mm the efficiency is recorded as 87.06 %.

Because of the page limitation further explanation of the motor optimization and analyze stages are not provided here.

V. CONCLUSIONS

This paper presents a structural integrity investigation of two-pole LS-SynRM with a new non-circular shaft structure. Unlike machines with 4 or more poles, the rotor flux path of 2 pole machines is disrupted by the shaft. To enhance the performance of the two-pole LS-SynRM, instead of standard circular shaft, a non-circular structure that narrows down the shaft along q-axis to expand the flux paths and upgrade the machine performance. Here, to ensure safe operation and prevent undesirable vibrations and deformations, a series of structural analysis is conducted to identify the appropriate dimensional limits.

The motor undergoes a structural analysis in three stages. Initially, modal analysis is conducted to calculate the natural frequencies at various reduction dimensions, enabling a safe limit for the reduction on shaft size to be determined and avoiding resonance-induced vibrations. Secondly, the maximum stress and deformation are calculated through harmonic analysis, accounting for manufacturing effects in the geometry. Finally, reduced shaft structure is checked if it can withstand the startup torque with static structural analysis. The rotor experienced five times the nominal value of the torque during the analyses.

Modal analysis using ANSYS Structural is conducted to identify the natural vibration modes and potential eccentricity as a result of the manufacturing imperfections is considered. The analysis concludes that the D_{OS} should be limited to 8 mm since the 1st NF appears at 146.6 Hz, which is far from twice the excitation frequency. Next, the stress and deformation under various excitation frequency conditions of the material at different excitation frequencies are investigated. The maximum acceptable D_{OS} limit is found to be 8 mm, where the maximum calculated deformation is 0.0389 mm, which is significantly less than the motor's airgap length of 0.35 mm. The last step is to conduct a shear stress analysis on the shaft when it's stationary and subject to five times the rated torque. Accordig to the results, the proposed shaft structure is found to be safe to operate when D_{OS} length is 8 mm. Accordingly, the efficiency of the LS-SynRM analyses results with circular shaft is obtained as 85.81 % while efficiency of the model with reduced shaft size along the q-axis (D_{OS}= 8 mm) is recorded as 87.06 %.

Future works may include a design methodology of the non-circular shaft LS-SynRM as bore-well pump motor with an extended investigation on electromagnetic and structural properties.

ACKNOWLEDGMENT

The research presented in this paper has received funding support from The Scientific and Technological Research Council of Turkey (TUBITAK) with Grant Number 121E413.

REFERENCES

[1] T. A. Lipo, *Introduction to AC Machine Design*. Hoboken, NJ, USA: John Wiley & Sons, Inc., 2017. doi: 10.1002/9781119352181.

[2] B. Stoffel, "The Role of Pumps for Energy Consumption and Energy Saving," *Assessing the Energy Efficiency of Pumps and Pump Units*, pp. 1–24, 2015, doi: 10.1016/B978-0-08-100597-2.00001-X.

[3] A. T. De Almeida, F. J. T. E. Ferreira, and G. Baoming, "Beyond induction motors - Technology trends to move up efficiency," *IEEE Trans Ind Appl*, vol. 50, no. 3, pp. 2103–2114, 2014, doi: 10.1109/TIA.2013.2288425.

[4] Y. Duan and D. M. Ionel, "A Review of Recent Developments in Electrical Machine Design Optimization Methods With a Permanent-Magnet Synchronous Motor Benchmark Study," *IEEE Trans Ind Appl*, vol. 49, no. 3, pp. 1268–1275, 2013, doi: 10.1109/TIA.2013.2252597.

[5] D. Mingardi and N. Bianchi, "Line-Start PM-Assisted Synchronous Motor Design, Optimization, and Tests," *IEEE Transactions on Industrial Electronics*, vol. 64, no. 12, 2017, doi: 10.1109/TIE.2017.2711557.

[6] A. Credo, G. Fabri, M. Villani, and M. Popescu, "A Robust Design Methodology for Synchronous Reluctance Motors," *IEEE*

Transactions on Energy Conversion, vol. 35, no. 4, pp. 2095–2105, Dec. 2020, doi: 10.1109/TEC.2020.3016567.

[7] A. Kersten, "Efficiency Investigation of Line Start Synchronous Reluctance Motors," 2017.

[8] Y. Hu, B. Chen, Y. Xiao, J. Shi, X. Li, and L. Li, "Rotor Design and Optimization of a Three-Phase Line-Start Synchronous Reluctance Motor," *IEEE Trans Ind Appl*, vol. 57, no. 2, pp. 1365–1374, 2021, doi: 10.1109/TIA.2020.3043224.

[9] M. Gamba, G. Pellegrino, A. Vagati, and F. Villata, "Design of a line-start synchronous reluctance motor," in *2013 International Electric Machines & Drives Conference*, IEEE, May 2013, pp. 648–655. doi: 10.1109/IEMDC.2013.6556163.

[10] Y. Hu, B. Chen, Y. Xiao, J. Shi, and L. Li, "Study on the Influence of Design and Optimization of Rotor Bars on Parameters of a Line-Start Synchronous Reluctance Motor," *IEEE Trans Ind Appl*, vol. 56, no. 2, pp. 1368–1376, 2020, doi: 10.1109/TIA.2019.2962431.

[11] A. Kersten, Y. Liu, D. Pehrman, and T. Thiringer, "Rotor design of line-start synchronous reluctance machine with round bars," *IEEE Trans Ind Appl*, vol. 55, no. 4, pp. 3685–3696, 2019, doi: 10.1109/TIA.2019.2914010.

[12] M. Villani, M. Santececca, and F. Parasiliti, "High-Efficiency Line-Start Synchronous Reluctance Motor for Fan and Pump Applications," *Proceedings - 2018 23rd International Conference on Electrical Machines, ICEM 2018*, pp. 2178–2184, 2018, doi: 10.1109/ICELMACH.2018.8507230.

[13] S. Baka, S. Sashidhar, and B. G. Fernandes, "Multi-barrier two-pole line-start synchronous reluctance motor with high saliency for a bore-well submersible pump," *Proceedings of the IEEE International Conference on Industrial Technology*, vol. 2018-Febru, pp. 475–480, 2018, doi: 10.1109/ICIT.2018.8352223.

[14] D. Tekgun and I. Alan, "A new oval shaft, high performance, 2 pole line start synchronous reluctance machine for submersible pump applications," *International Journal of Applied Electromagnetics and Mechanics*, vol. Preprint, no. Preprint, pp. 1–21, Jun. 2022, doi: 10.3233/JAE-220026.

[15] D. Tekgun, M. Muhsin Cosdu, B. Tekgun, and I. Alan, "Investigation of the Effects of Multi-Layer Winding Structures in Two Pole Synchronous Reluctance Machines," *Proceedings - 2021 IEEE 3rd Global Power, Energy and Communication Conference, GPECOM 2021*, pp. 120–125, Oct. 2021, doi: 10.1109/GPECOM52585.2021.9587567.

[16] D. Tekgun, M. Muhsin Cosdu, B. Tekgun, and I. Alan, "Effect of the Stator Slot Indents on Fluid Damping Loss in Submersible Pump Applications; Effect of the Stator Slot Indents on Fluid Damping Loss in Submersible Pump Applications," *2022 4th Global Power, Energy and Communication Conference (GPECOM)*, 2022, doi: 10.1109/GPECOM55404.2022.9815636.

[17] D. Tekgun, B. Tekgun, and I. Alan, "FEA based fast topology optimization method for switched reluctance machines," *Electrical Engineering*, pp. 1–11, Jan. 2022, doi: 10.1007/S00202-021-01453-9/FIGURES/8.

[18] Anup Kumar Dey, "What Is Modal Analysis and Why Is It Necessary? (With PDF) – What Is Piping." https://whatispiping.com/modal-analysis/ (accessed Dec. 29, 2022).

[19] E. C. Lovelace, T. M. Jahns, T. A. Keim, and J. H. Lang, "Mechanical design considerations for conventionally laminated, high-speed, interior PM synchronous machine rotors," *IEEE Trans Ind Appl*, vol. 40, no. 3, pp. 806–812, May 2004, doi: 10.1109/TIA.2004.827440.